ACS APPLIED MATERIALS & INTERFACES

Research Article

www.acsami.org

Highly Dense ZnO Nanowires Grown on Graphene Foam for Ultraviolet Photodetection

Buddha Deka Boruah, Anwesha Mukherjee, S. Sridhar, and Abha Misra*

Department of Instrumentation and Applied Physics, Indian Institute of Science, Bangalore, Karnataka, India 560012

ABSTRACT: Growth of highly dense ZnO nanowires (ZnO NWs) is demonstrated on three-dimensional graphene foam (GF) using resistive thermal evaporation technique. Photoresponse of the as-grown hybrid structure of ZnO NWs on GF (ZnO NWs/GF) is evaluated for ultraviolet (UV) detection. Excellent photoresponse with fast response and recovery times of 9.5 and 38 s with external quantum efficiency of 2490.8% is demonstrated at low illumination power density of 1.3 mW/cm^2. In addition, due to excellent charge carrier transport, mobility of graphene reduces the recombination rate of photogenerated charge carriers, hence the lifetime of photogenerated free charge carriers enhances in the photodetectors.

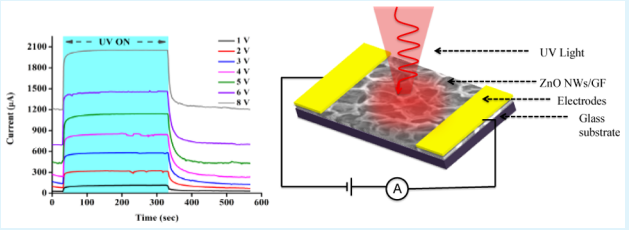

KEYWORDS: *Zinc oxide, nanowire, graphene foam, heterostructure, photodetector*

INTRODUCTION

Zinc oxide (ZnO) is a promising semiconducting material due to its unique optical and electrical properties.[1,2] For instance, ZnO has a wide direct band gap of 3.37 eV and also exhibits large exciton binding energy of 60 meV which is much larger than the room-temperature thermal energy (26 meV). Hence, ZnO material is broadly employed in various applications such as electronic and optoelectronic devices,[3,4] chemical sensors,[5] and biosensors,[6] etc. Among these, ZnO is highly used in ultraviolet (UV) photodetectors and due to large surface-to-volume ratio ZnO nanowires (NWs) are highly preferable. Moreover, UV photodetectors based on different ZnO heterostructures are used to improve the device parameters such as response time, recovery time, responsivity, and external quantum efficiency.[7,8] Still, research continues to develop novel ZnO-based heterostructures for further improvement in photoresponses of UV photodetectors. Recently, graphene, a two-dimensional carbon monolayer has attracted much attention in electronics and optoelectronic devices because of excellent charge carriers transport mobility, high electrical conductivity, and mechanical flexibility.[9−11] In addition, graphene is prominently used with semiconducting oxide materials to improve the performance of optoelectronic devices.[12,13] Three-dimensional microstructure of graphene due to high surface area in the form of graphene foam (GF) could be an excellent choice in conjunction with highly dense ZnO NWs for optoelectronic devices, for example UV photodetector.

This report presents the growth of highly dense ultrathin ZnO NWs on GF (ZnO NWs/GF) by resistive thermal evaporation (RTE) process for the photodetector. A UV photodetector based on hybrid structure of ZnO NWs/GF is fabricated with an active area of 3 × 3 mm^2. The hybrid structure of ZnO NWs/GF-based UV photodetector demonstrated high external quantum efficiency with faster response and recovery times upon exposure to much lower illumination power density as compared to ZnO nanostructures that will be discussed later.

RESULTS AND DISCUSSION

Figure 1 illustrates a schematic diagram of experimental steps involved in the synthesis of the hybrid structure. Further details

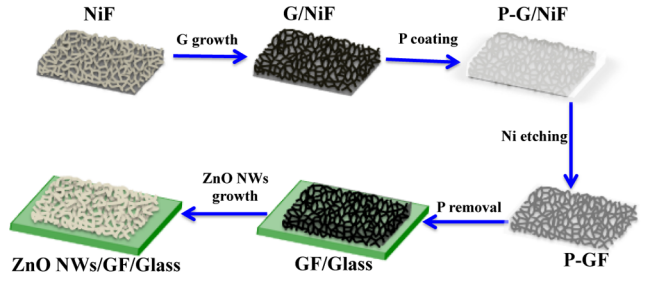

Figure 1. Schematic of steps involved in preparation of sample.

are provided in the Experimental Section. Figure 2a shows a low-magnification scanning electron microscopy (SEM) image of GF after etching nickel substrate, where a uniform growth of graphene on the substrate can be seen and the original open cell-like structure remains intact. The inset demonstrates a high-magnification image of GF surface. Grain boundaries on graphene are clearly visible; they originated due to the lattice

Received: March 18, 2015
Accepted: April 27, 2015
Published: April 27, 2015

DOI: 10.1021/acsami.5b02403
ACS Appl. Mater. Interfaces 2015, 7, 10606−10611

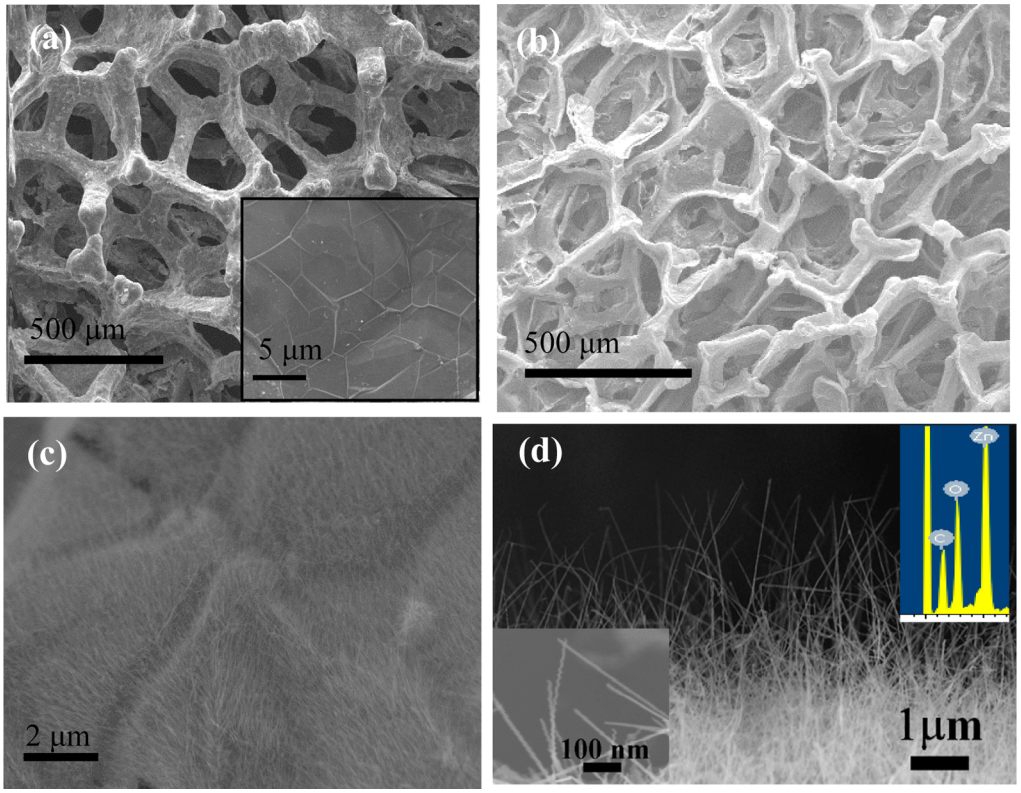

Figure 2. SEM images of (a) GF at low magnification and high magnification (inset), (b) ZnO NWs on GF at low magnification, (c) ZnO NWs uniformly grown on GF, and (d) high-magnification image of ZnO NWs; left inset demonstrates further resolved SEM image of NWs and right inset is an EDS spectrum of ZnO NWs/GF sample.

mismatch between graphene and nickel, which is also observed in other reports.[14,15] Figure 2b shows a low-magnification SEM image of the ZnO NWs grown onto the GF surface, where a uniform coating is clearly visible everywhere on the GF. Figure 2c shows a high-resolution image of highly dense ZnO NWs uniformly grown on GF. Figure 2d demonstrates a further magnified image of conformal ZnO NWs with the diameter ranging from 10 to 30 nm and length in the range of a few microns (left inset). Energy dispersive spectroscopy (EDS) was performed on ZnO NWs/GF that reveals the presence of zinc, oxygen, and carbon only, hence presenting the absence of any other impurity as shown in the right inset.

Growth of the ZnO NWs on GF can be understood from the well-known vapor−solid mechanism, where the evaporated Zn vapors react with oxygen to form ZnO and deposited on the desired substrate. The temperature gradient induces the deposited ZnO to form ZnO NWs.[16]

Figure 3 reveals an X-ray diffraction (XRD) pattern of ZnO NWs/GF. Diffraction peaks of graphene (indicated by G) appear at 2θ = 26.48° and 54.71°, which indicate the presence of (002) and (004) crystalline planes of graphene.[17] The diffraction peaks of ZnO also appear at 2θ = 31.71°, 34.4°, 36.30°, 47.52°, 56.6°, 62.9°, 66.3°, 72.5°, and 77.0°. These peaks indicate the hexagonal wurtzite crystal structure of ZnO with planes (100), (002), (101), (102), (110), (103), (200), (004), and (202), respectively.[18] Peaks at around 2θ = 32.94° and 69.13° represent (200) and (400) planes of silicon, which was used as a substrate to conduct the XRD characterizations.[19] Therefore, XRD analysis reveals a high crystal quality of ZnO NWs on GF.

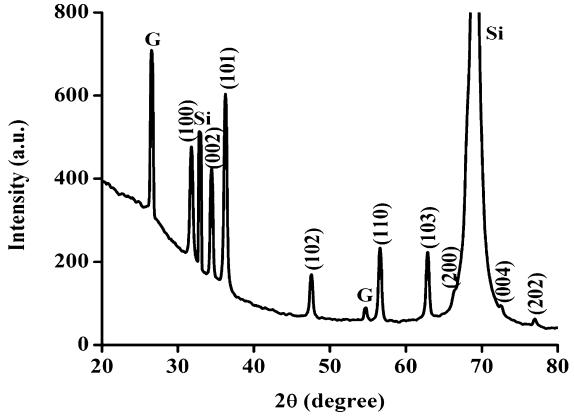

Figure 3. XRD spectrum of as-grown ZnO NWs on GF.

Results of Raman analysis of GF and ZnO NWs/GF are shown in Figure 4a and b. Raman peaks at 1358, 1575, and 2702 cm^{-1} represent D, G, and 2D bands of graphene. In both GF and as-grown ZnO NWs on GF, a weaker intensity of D band is shown as compared to G and 2D bands, which is the signature of presence of crystalline graphene as described by Graf et al.[20] A few defects in graphene could arise from the wrinkling at the grain boundaries as shown earlier in Figure 2. The peak intensity ratio of G to 2D band is 1.16, which represents the few-layer graphene.[14,20] Additional peaks in Raman spectrum of as-grown ZnO NWs on GF at 439 and 562.7 cm^{-1} represent A_1 longitudinal optical (LO) and E_2 (high) modes of ZnO wurtzite structure (Figure 4b).[21,22]

The electrical measurements under UV illumination were conducted on ZnO NWs/GF sample by using conducting silver

DOI: 10.1021/acsami.5b02403
ACS Appl. Mater. Interfaces 2015, 7, 10606−10611

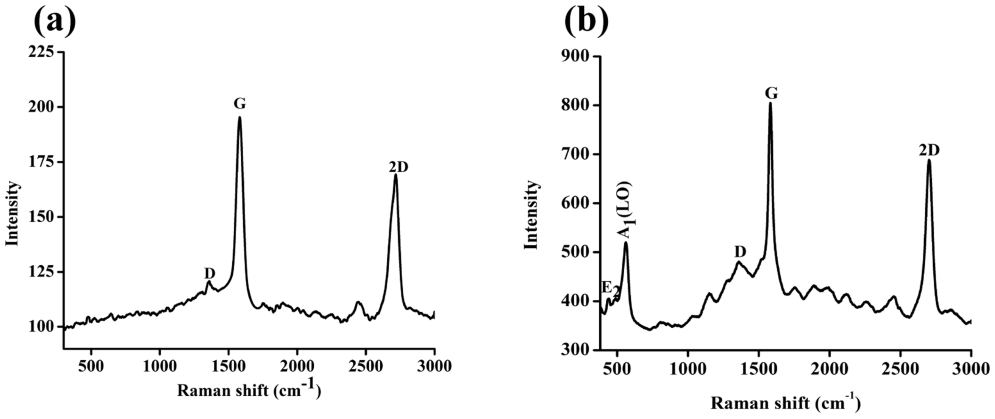

Figure 4. (a) Raman spectra of GF and (b) as-grown ZnO NWs on GF.

paste for the electrodes and the distance between electrodes was maintained 3 mm. This distance was chosen to avoid any electrical shorting of the device. The schematic of ZnO NWs/GF device is shown in Figure 5.

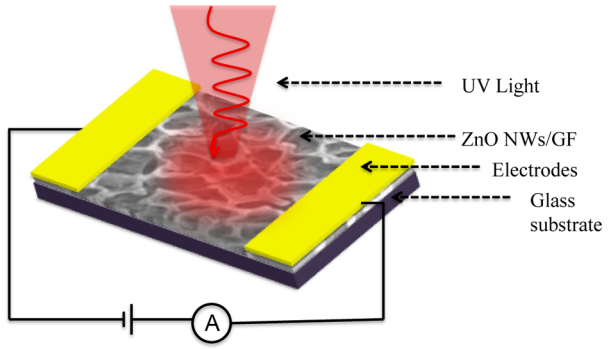

Figure 5. Schematic of ZnO NWs/GF device.

Figure 6a shows the current−voltage (I−V) response of ZnO NWs/GF device both in absence and presence of UV illumination. Both the plots given in Figure 6a show an asymmetric behavior of both the dark current (in the absence of UV illumination) and the photocurrent (in the presence of UV illumination) with the variation in bias voltage. The appearance of the asymmetric I−V could be related to the formation of nearly Ohmic contact between ZnO NWs and silver paint.[23] Also both the plots reveal higher photocurrent than the dark current at a particular bias voltage. The photoresponse of ZnO NWs could be attributed to the fact that in the absence of UV illumination a low conductivity depletion layer forms on the surface due to adsorption of oxygen molecules from the ambient air that captures free electrons from n-type ZnO NWs. Under UV illumination, electron−hole pairs are generated with energy higher than or equal to the band gap of ZnO and cause desorption of oxygen molecules due to the trapping of generated free holes by oxygen ions present onto the surface. A decrease in the depletion layer results in an increase in free charge carrier concentrations, which enhances the conductivity of the device.[24,25] Furthermore, in ZnO NWs/GF device as shown in Figure 5, conduction of charge carriers takes place mainly through ZnO NWs-GF-ZnO NWs due to highly dense growth of ZnO NWs on GF. However, conduction through graphene layer will mainly contribute to the generation of dark current.[26] Hence, upon UV exposure, the photogenerated free charge carriers are transferred from ZnO NWs to graphene layers of the foam, and higher charge carrier mobility of graphene induces a faster collection of the charge carriers at the electrode with longer lifetime by reducing the charge recombination rate.

Switching photoresponse of ZnO NWs/GF device for eight cycles of turning on and off the UV illumination is measured at a bias voltage of 5 V as shown in Figure 6b. The measured current is plotted with the exposure time. In addition, the device demonstrated repeatable response over all the exposure cycles. Figure 6c reveals the photoresponse of the device at a bias voltage of 5 V for a continuous illumination of UV until the response saturates. The response time (t_{res}) is defined as the time required for the current to reach from 10 to 90% of its maximum value[12] and recovery time (t_{rec}) is defined as the time required by the current to fall from 90 to 10% from the maximum value.[12] The measured values are 9.5 and 38 s, respectively, which shows a significant improvement in response and recovery times as compared to previously reported ZnO nanostructure-based UV photodetectors, where response and recovery times vary from 50 to 500 s.[27−31] The reason behind the longer recovery time is as follows: generally in ZnO nanostructure-based UV photodetectors, the response and recovery times of the device are mainly determined by oxygen desorption and absorption processes. Upon UV illumination in ZnO NWs/GF device, when oxygen desorption takes place, the generated free charge carriers transferred to graphene and quickly get saturated within small response time of 9.5 s as described earlier. After switching off the UV illumination, until the oxygen molecules capture all the photogenerated free charge carriers, they continue contributing to the current in the device. The process of absorption of oxygen molecules from air takes a longer time as compared to the desorption process.[32] Therefore, observed recovery time is longer than response time.

The variation of differential conductivity (dI/dV) of ZnO NWs/GF device with the bias voltage is shown in Figure 6d under both the presence and absence of UV illumination. At zero bias voltage, the dark differential conductivity $(dI/dV)_D$ (in absence of UV) and photo differential conductivity $(dI/dV)_P$ (in the presence of UV) are 50.5 and 80.5 μS, respectively, which shows nearly 60% enhancement in $(dI/dV)_P$ as compared to $(dI/dV)_D$ because of the above-described charge transport mechanism upon UV illumination. It is observed that both $(dI/dV)_P$ and $(dI/dV)_D$ gradually increase with bias voltage and demonstrate an asymmetric behavior that could be

DOI: 10.1021/acsami.5b02403
ACS Appl. Mater. Interfaces 2015, 7, 10606−10611

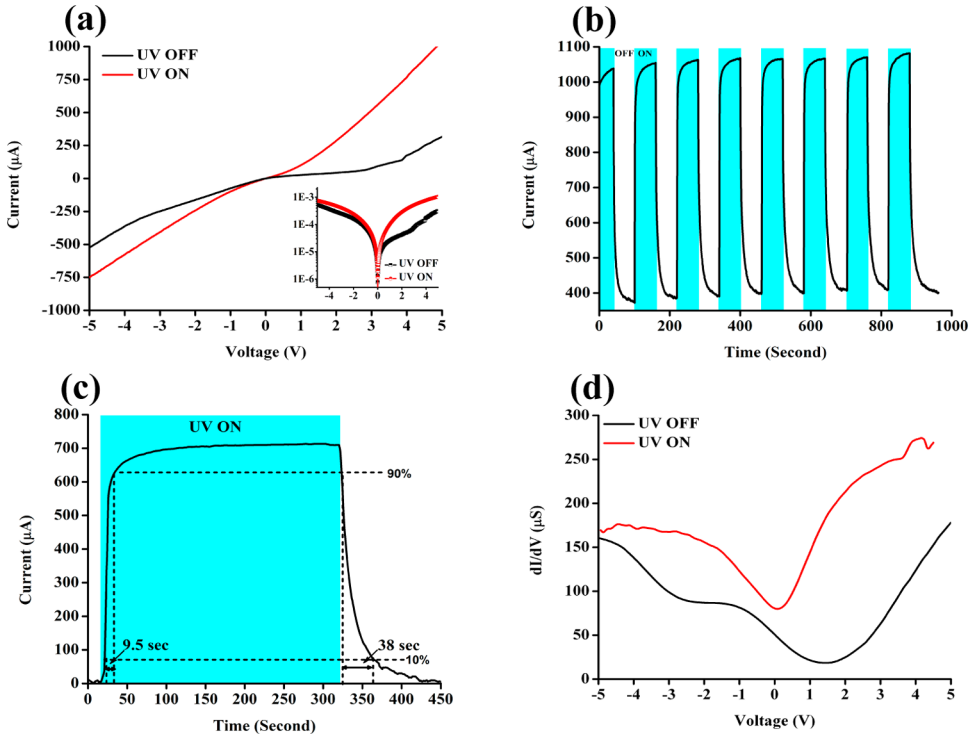

Figure 6. (a) *I*−*V* response of ZnO NWs/GF device in the presence and absence of UV illumination and inset shows a log plot of current. (b) Cyclic photoresponse of the device. (c) Saturation response of the device to calculate response time and recovery time. (d) Differential conductivity (d*I*/d*V*) of the device plotted with the bias voltage.

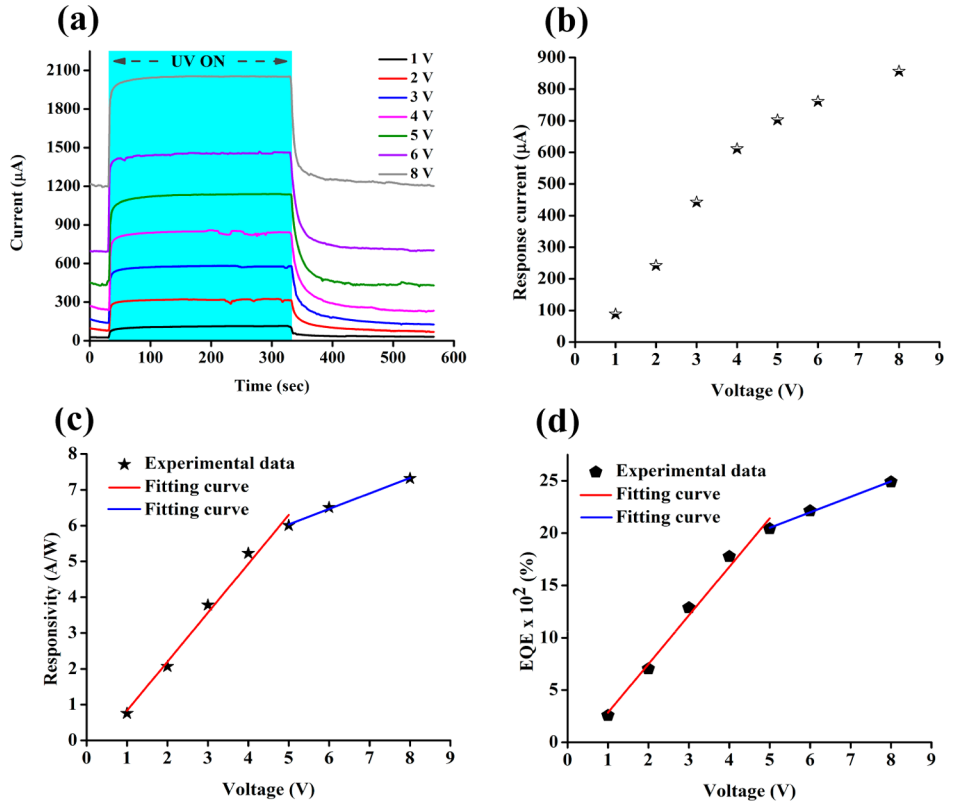

Figure 7. (a) Saturation experiments at different bias voltage, (b) response current at different bias voltage. Dependence of (c) responsivity and (d) external quantum efficiency of ZnO NWs/GF device with bias voltage.

DOI: 10.1021/acsami.5b02403
ACS Appl. Mater. Interfaces 2015, 7, 10606−10611

again related to the formation of nearly Ohmic contact. The device shows almost 56% enhancement of $(dI/dV)_p$ that of $(dI/dV)_D$ at 5 V bias voltage.

Furthermore, the photoresponse of the device in saturation was monitored with the varying bias voltage from 1 to 8 V as shown in Figure 7a. The plot shows that the photoresponse is a function of bias voltage and increases with the applied bias. Response current ($I = I_{UV} - I_{dark}$), where I_{UV} and I_{dark} represent currents in the presence and absence of UV illumination, is calculated from Figure 7a and reveals that the response current is a function of bias voltage as shown in Figure 7b. At a maximum applied bias voltage of 8 V, response current increases approximately by ~868% as compared to lowest applied bias voltage of 1 V. Response current values are further used for the evaluation of device parameters, namely responsivity and external quantum efficiency of ZnO NWs/GF device. The responsivity (R_s) is defined as the ratio of the response current to the illumination power on photodetector as given by

$$R_s = \frac{I}{P_o A} \tag{1}$$

where P_o is the UV illumination power density, and A is the active device area.[33] Figure 7c shows a dependence of R_s on bias voltage in two stages. In the range 1−5 V, it can be clearly observed that the value of R_s increases linearly with the bias voltage that can be fitted with a straight line of slope ~1.4 (A/W)V^{-1}. However, in the region of 5−8 V, the values of R_s can be fitted with another straight line with a lower slope of 0.43 (A/W)V^{-1}. The difference in the slope of fitted lines for two different ranges of bias voltage reveals the occurrence of phonon scattering and self-generating heat in the larger voltage region due to which the increment in I_{dark} with bias voltage is more and hence the response current becomes less.[34,35] At a bias voltage of 5 V, the enhancement of R_s is 694% as compared to a bias voltage of 1 V, and at the bias voltage of 8 V, only 22% enhancement of R_s is observed as compared to a 5 V bias voltage.

Furthermore, the external quantum efficiency (EQE) of the photodetector is calculated, which is defined as the number of charge carriers generated per number of incident photons on the device as given by the following relation:

$$\mathrm{EQE} = \frac{R_s}{(q/h\upsilon)} \times 100 \tag{2}$$

where q is the elementary charge, υ is the frequency of absorbed photon, and h is Planck's constant.[36]

Dependence of EQE of ZnO NWs/GF device with the applied bias voltage is revealed in Figure 7d. The EQE of the device linearly increases with the rate of 4.64×10^2% V^{-1} in the range of 1−5 V. Similarly, in the range of 5−8 V, the rate of increase in EQE is 1.5×10^2% V^{-1} which is relatively lesser as compared to lower bias voltage region. In the large bias voltage range, the rate of increment of I is less due to more phonon scattering and self-generating heat in the device as mentioned earlier. Calculated EQE values at bias voltages of 1, 5, and 8 V are 257%, 2042%, and 2491%, respectively.

CONCLUSION

Highly dense ultrathin ZnO NWs growth on GF by a simple and fast RTE technique is reported. The fabricated ZnO NWs/GF device shows an excellent UV photoresponse with fast response and recovery times as compared to previously reported ZnO nanostructure-based UV photodetectors. The present device shows excellent EQE, where these values are 257.5%, 2041.6%, and 2490.8% at the applied bias voltages of 1, 5, and 8 V, respectively.

EXPERIMENTAL SECTION

Atmospheric chemical vapor deposition was carried out on nickel foam to synthesize GF with an area of 5 × 3 mm^2. Initially, nickel foam was cleaned with isopropyl alcohol and deionized water and then dried using nitrogen gas. The cleaned substrate was then kept inside a high-temperature horizontal tube furnace (1000 °C) under a constant flow of argon gas for inert atmosphere. Before graphene growth, the nickel substrate was annealed for 15 min in the presence of both hydrogen and argon gases to remove the native oxide from nickel surface. Subsequently, growth of GF was conducted for 2.5 min by introducing methane gas. A detailed synthesis procedure of GF on the surface of nickel foam can be found elsewhere.[14] Freestanding GF was achieved by first coating the as-grown sample with poly(bisphenol carbonate) (PC) and then dried in air at 80 °C for 60 min, followed by dipping the sample into 3 M HCl kept at 120 °C for 12 h for etching of nickel. After nickel etching, the sample was washed with deionized water and then dipped into chloroform for 60 min to remove the PC. The nickel- and PC-free GF sample was then transferred onto a cleaned substrate and dried at 110 °C for 60 min in air. Thereafter, GF was placed inside the RTE chamber to grow ZnO NWs, where RTE chamber was evacuated to 2×10^{-5} mbar pressure using rotary and diffusion pumps. Granulated zinc was evaporated onto the GF by resistive heating of the tantalum boat placed 2 cm apart from the substrate. During the ZnO NWs growth, oxygen gas was allowed into the chamber while maintaining a chamber pressure of 8×10^{-4} mbar for 5 min.

Surface morphology and crystal structure of ZnO NWs/GF were investigated using SEM (FEI Sirion XL30 FEG SEM) at an acceleration voltage of 10 kV, and XRD) (Rigaku, Smart lab) with a scan rate of 2°/min using Cu$K\alpha_1$ as a source. EDS (Detector EDAX Genesis) was performed for the analysis of elemental composition of sample. Raman analysis (Horiba Jobin Yvon LabRAM HR) was performed to confirm the quality of the ZnO-deposited graphene. The Raman spectrometer was used with a laser wavelength of 532 nm. UV radiation source (Philips TL-D 18 W) of 1.3 mW/cm^2 power density with a wavelength of 365 nm was used to study the photoresponse of the fabricated ZnO NWs/GF device. A change in current was measured upon UV exposure while applying a constant bias voltage. Current−voltage (I−V) characteristic of the device was acquired by sweeping the bias voltage from −5 to +5 V both in the presence and absence of UV using a Keithley 2611B source-meter system. The cyclic response of the device was performed for eight continuous cycles of UV radiation, and each cycle UV was illuminated for 1 min at a fixed bias voltage of 5 V. Photo response parameters such as response time, recovery time, responsivity, and external quantum efficiency of device were estimated while performing photoresponse saturation experiments at different bias voltages.

AUTHOR INFORMATION

Corresponding Author

*E-mail: abha.misra1@gmail.com.

Notes

The authors declare no competing financial interest.

REFERENCES

(1) Wang, Z. L. Zinc Oxide Nanostructures: Growth, Properties and Applications. *J. Phys.: Condens. Matter* **2004**, *16*, R829−R858.

(2) Fan, Z.; Lu, J. G. Zinc Oxide Nanostructures: Synthesis and Properties. *J. Nanosci. Nanotechnol.* **2005**, *10*, 1561−1573.

(3) Djurisic, A. B.; Ng, A. M. C.; Chen, X. Y. ZnO Nanostructures for Optoelectronics: Material Properties and Device Applications. *Prog. Quantum Electron.* **2010**, *34*, 191−259.

DOI: 10.1021/acsami.5b02403
ACS Appl. Mater. Interfaces 2015, 7, 10606−10611

(4) Sakurai, M.; Wang, Y. G.; Uemura, T.; Aono, M. Electrical Properties of Individual ZnO Nanowires. *Nanotechnology* **2009**, *20*, 15520−155208.
(5) Umar, A.; Rahman, M. M.; Kim, S. H.; Hahn, Y.-B. Zinc Oxide Nanonail Based Chemical Sensor for Hydrazine Detection. *Chem. Commun.* **2008**, *2*, 166−168.
(6) Kumur, N.; Dorfman, A.; Hahm, J.-I. Ultrasensitive DNA Sequence Detection Using Nanoscale ZnO Sensor Arrays. *Nanotechnology* **2006**, *17*, 2875−2881.
(7) Tian, W.; Zhai, T.; Zhang, C.; Li, S.-L.; Wang, X.; Liu, F.; Liu, D.; Cai, X.; Tsukagosh, K.; Golberg, D.; Bando, Y. Low-Cost Fully Transparent Ultraviolet Photodetectors Based on Electrospun ZnO-SnO_2 Heterojunction Nanofibres. *Adv. Mater.* **2013**, *25*, 4625−4630.
(8) Ok, J. G.; Lee, J. Y.; Baac, H. W.; Tawfick, S. H.; Guo, L. J.; Hart, A. J. Rapid Anisotropic Photoconductive Response of ZnO-Coated Aligned Carbon Nanotube Sheets. *ACS Appl. Mater. Interfaces* **2014**, *6*, 874−881.
(9) Bonaccorso, F.; Sun, Z.; Hasan, T.; Ferrari, A. C. Graphene Photonics and Optoelectronics. *Nat. Photonics* **2010**, *4*, 611−622.
(10) Geim, A. K. Graphene: Status and Prospects. *Science* **2009**, *324*, 1530−1534.
(11) Geim, A. K.; Novoselov, K. S. The Rise of Graphene. *Nat. Mater.* **2007**, *6*, 183−191.
(12) Nie, B.; Hu, J.-G.; Luo, L.-B.; Xie, C.; Zeng, L.-H.; Lv, P.; Li, F.-Z.; Jie, J.-S.; Feng, M.; Wu, C.-Y.; Yu, Y.-Q.; Yu, S.-H. Monolayer Graphene Film on ZnO Nanorod Array for High-Performance Schottky Junction Ultraviolet Photodetectors. *Small* **2013**, *9*, 2872−2879.
(13) Fu, X.-W.; Liao, Z.-M.; Zhou, Y.-B.; Wu, H.-C.; Bie, Y.-Q.; Xu, J.; Yu, D.-P. Graphene/ZnO Nanowire/Graphene Vertical Structure Based Fast-Response Ultraviolet Photodetector. *Appl. Phys. Lett.* **2012**, *100*, 223114−223117.
(14) Reddy, S. K.; Ferry, D. B.; Misra, A. Highly Compressible Behavior of Polymer Mediated Three-Dimensional Network of Graphene Foam. *RSC Adv.* **2014**, *4*, 50074−50080.
(15) Yavari, F.; Chen, Z.; Thomas, A. V.; Ren, W.; Cheng, H.-M.; Koratkar, N. High Sensitivity Gas Detection Using a Macroscopic Three-Dimensional Graphene Foam Network. *Sci. Rep.* **2011**, *1*, 1−5.
(16) Hsu, Y.-J.; Lu, S. Y. Vapor-Solid Growth of Sn Nanowires: Growth Mechanism and Supercoductivity. *J. Phys. Chem. B* **2005**, *109*, 4398−4403.
(17) Dong, X.; Cao, Y.; Wang, J.; Chen-Park, M. B.; Wang, L.; Huang, W.; Chen, P. Hybrid Structure of Zinc Oxide Nanorods and Three Dimensional Graphene Foam for Supercapacitor and Electrochemical Sensor Applications. *RSC Adv.* **2012**, *2*, 4364−4369.
(18) Yang, P.; Yan, H.; Mao, S.; Russo, R.; Johnson, J.; Saykally, R.; Morris, N.; Pham, J.; He, R.; Choi, H.-J. Controlled Growth of ZnO Nanowires and Their Optical properties. *Adv. Funct. Mater.* **2012**, *12*, 323−331.
(19) Tian, L.; Ouyang, T.; Loh, K. P.; Vittal, J. J. La_2S_3 Thin Films from Metal Organic Chemical Vapor Deposition of Single-Source Precursor. *J. Mater. Chem.* **2006**, *16*, 272−277.
(20) Graf, D.; Molitor, F.; Ensslin, K.; Stampfer, C.; Jungen, A.; Hierold, C.; Wirtz, L. Spatially Resolved Raman Spectroscopy of Single- and Few-Layer Graphene. *Nano Lett.* **2007**, *7*, 238−242.
(21) Ye, J.; Gu, S.; Zhu, S.; Chen, T.; Liu, W.; Qin, F.; Hu, L.; Zhang, R.; Shi, Y.; Zheng, Y. Raman and Photoluminescence of ZnO Films Deposited on Si (111) Using Low-Pressure Metalorganic Chemical Vapor Deposition. *J. Vac. Sci. Technol. A* **2003**, *21*, 979−982.
(22) Yang, L.; Yang, J.; Wang, D.; Zhang, Y.; Wang, Y.; Liu, H.; Fan, H.; Lang, J. Photoluminescence and Raman Analysis of ZnO Nanowires Deposited on Si (100) Via Vapor-Liquid-Solid Process. *Phys. E (Amsterdam, Neth.)* **2008**, *40*, 920−923.
(23) Yan, F.; Wang, Y.; Zhang, J.; Liu, Z.; Zheng, J.; Huang, F. Schottky or Ohmic Metal-Semiconductor Contact: Influence on Photocatalystic Efficiency of Ag/ZnO and Pt/ZnO Model Systems. *ChemSusChem* **2014**, *7*, 101−104.
(24) Kind, H.; Yan, H.; Messer, B.; Law, M.; Yang, P. Nanowire Ultraviolet Photodetectors and Optical Switches. *Adv. Mater.* **2002**, *14*, 158−160.
(25) Takahashi, Y.; Kanamori, M.; Kondoh, A.; Minoura, H.; Ohya, Y. Photoconductivity of Ultrathin Zinc Oxide Films. *Jpn. J. Appl. Phys.* **1994**, *33*, 6611−6615.
(26) Koppens, F. H. L.; Mueller, T.; Avouris, Ph.; Ferrari, A. C.; Vitiello, M. S.; Polini, M. Photodetectors Based on Graphene, Other Two-Dimensional Materials and Hybrid Systems. *Nat. Nanotechnol.* **2014**, *9*, 768−793.
(27) Manekkathodi, A.; Lu, M.-Y.; Wang, C. W.; Chen, L.-J. Direct Growth of Aligned Zinc Oxide Nanorods on Paper Substrates for Low-Cost Flexible Electronics. *Adv. Mater.* **2010**, *22*, 4059−4063.
(28) Liu, K.; Sakurai, M.; Liao, M.; Aono, M. Giant Improvement of the Performance of ZnO Nanowire Photodetectors by Au Nanoparticles. *J. Phys. Chem. C* **2010**, *114*, 19835−19839.
(29) Ahn, S.-E.; Ji, J. H.; Kim, K.; Kim, G. T.; Bae, C. H.; Park, S. M.; Kim, Y.-K.; Ha, J. S. Origin of the Slow Photoresponse in an Individual Sol-Gel Synthesized ZnO Nanowire. *Appl. Phys. Lett.* **2007**, *90*, 153106−153108.
(30) Hu, L.; Chen, M.; Shan, W.; Zhan, T.; Liao, M.; Fang, X.; Hu, X.; Wu, L. Stacking-Order-Dependent Optoelectronic Properties of Bilayer Nanofilm Photodetectors Made From Hollow ZnS and ZnO Microspheres. *Adv. Mater.* **2012**, *24*, 5872−5877.
(31) Bera, A.; Basak, D. Photoluminescence and Photoconductivity of ZnS-Coated ZnO Nanowires. *ACS Appl. Mater. Interfaces* **2010**, *2*, 408−412.
(32) Cheng, J.; Zhang, Y.; Guo, R. ZnO Microtube Ultraviolet Photodetector. *J. Cryst. Growth* **2008**, *310*, 57−61.
(33) Zhu, L.; Gu, X.; Qu, F.; Zhang, J.; Feng, C.; Zhou, J.; Ruan, S.; Kang, B. Electrospun ZnO Nanofibers-Based Ultraviolet Detector with High Responsivity. *J. Am. Ceram. Soc.* **2013**, *96*, 3183−3187.
(34) Vandecasteele, N.; Barreiro, A.; Lazzeri, M.; Bachtold, A.; Mauri, F. Current-voltage characteristics of graphene devices: Interplay between Zener-Klein tunneling and defects. *Phys. Rev. B* **2010**, *82*, 045416−45425.
(35) Popinciuc, M.; Calado, V. E.; Liu, X. L.; Akhmerov, A. R.; Klapwijk, T. M.; Vandersypen, L. M. K. Zero-bias conductance peak and Josephson effect in graphene-NbTiN junctions. *Phys. Rev. B* **2012**, *85*, 205404−205408.
(36) Wu, J. M.; Chang, W. E. Ultrahigh responsivity and External Quantum Efficiency of an Ultraviolet-Light Photodetector Based on a Single VO_2 Microwire. *ACS Appl. Mater. Interfaces* **2014**, *6*, 14286−14292.

DOI: 10.1021/acsami.5b02403
ACS Appl. Mater. Interfaces 2015, 7, 10606−10611